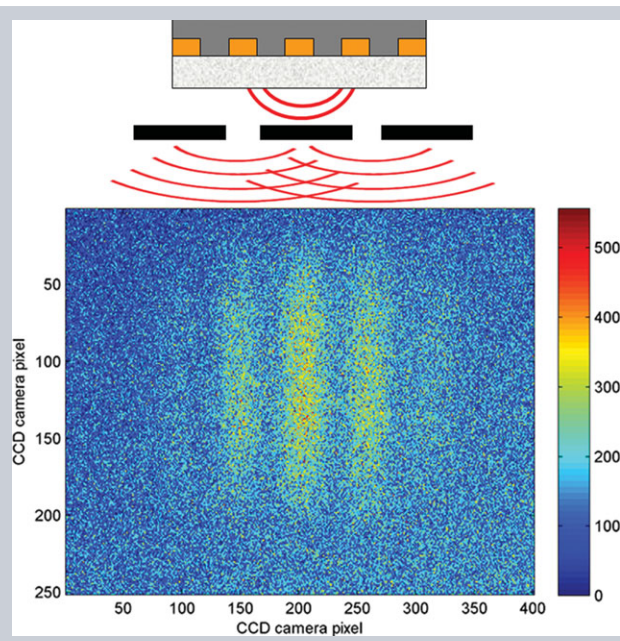


**Abstract** The spatial coherence of organic light-emitting diodes (OLEDs) is an important parameter that has gained little attention to date. Here, we present a method for making quantitative measurements of the spatial coherence of OLEDs using a Young's double-slit experiment. The usefulness of the method is demonstrated by making measurements on a range of OLEDs with different emitters (iridium and europium complexes) and architectures (bottom and top emitting) and the fringe visibility is further manipulated by gratings embedded in external diffractive optical elements. Based on the experiments and simulation of the results, we quantitatively determine the spatial coherence lengths of several OLEDs and find them to be a few micrometers. A 60% increase in the spatial coherence length was observed when using a narrow bandwidth emitter and a metal-coated grating.



## Measuring and structuring the spatial coherence length of organic light-emitting diodes

Guohua Xie<sup>1</sup>, Mingzhou Chen<sup>2</sup>, Michael Mazilu<sup>2</sup>, Shuyu Zhang<sup>1,3</sup>, A.K. Bansal<sup>1</sup>, Kishan Dholakia<sup>2</sup>, and Ifor D. W. Samuel<sup>1,\*</sup>

### 1. Introduction

Organic light-emitting diode (OLED) technology has attracted great attention due to its promising applications in lighting and displays [1–14]. Recently, new applications of this technology in visible-light communication and biomedical instruments suggest that OLEDs will be universal in the next generation of photonic devices [15–18]. For such emerging applications, the coherence of the beam and the ability to make it directional are of interest. OLEDs are compact, versatile, potentially low-cost and visible sources. Though many aspects of the electrical and optical properties of OLEDs have been studied in the last 25 years [7, 19–21], the spatial coherence has received very little attention. The microcavity-like structures used in OLEDs pave the way for optical management and manipulation [22–27]. This makes them ideal alternative light sources for portable and disposable instruments for biomedical applications such as photodynamic

therapy for skin-cancer treatment [18]. In this context, the spatial coherence of a light source is important for being able to shape and direct the emission beam – for example the wavefront of a beam of sufficient spatial coherence can be shaped by a spatial light modulator. The coherence also plays a large role in the penetration of light into living tissues [28–30].


Duarte et al. reported an investigation of the spatial coherence of an electrically driven OLED containing the laser dye 10-(2-benzothiazolyl)-1,1,7,7-tetramethyl-2,3,6,7-tetrahydro-1H,5H,11H-benzo[*l*]-pyrano[6,7,8-*ij*]quinolizin-11-one (C545T) as the emitting layer (EML), using a Young's double-slit experiment [31]. In their work, an additional single-slit was inserted between the OLED and the double slit. Therefore, the spatial distribution of the light beam after two spatial filters (two single slits) was modified dramatically, which contributed to a small beam divergence of 2.53 mrad and similar fringes to those from a He-Ne laser were observed. These are interesting results

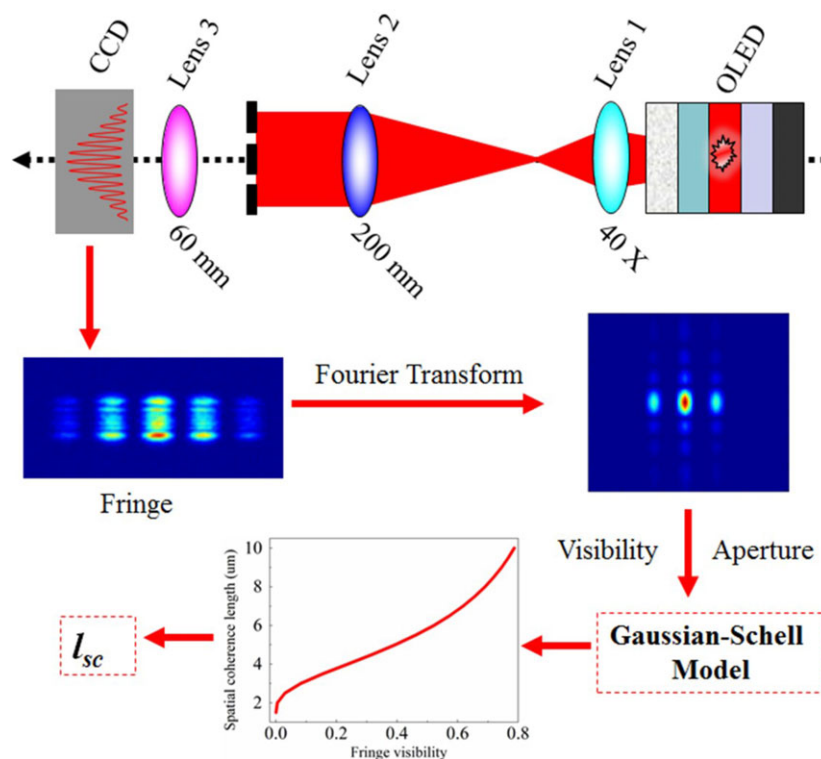
<sup>1</sup> Organic Semiconductor Centre, SUPA, School of Physics and Astronomy, University of St Andrews, North Haugh, St Andrews, KY16 9SS, UK

<sup>2</sup> SUPA, School of Physics and Astronomy, University of St Andrews, North Haugh, St Andrews, KY16 9SS, UK

<sup>3</sup> Present address: School of Information Science and Technology, Fudan University, North Haugh, Shanghai 200433, China

\*Corresponding author: [idws@st-andrews.ac.uk](mailto:idws@st-andrews.ac.uk)

 This is an open access article under the terms of the Creative Commons Attribution License, which permits use, distribution and reproduction in any medium, provided the original work is properly cited.



**SCHEME 1** The optical setup used to measure fringe visibility and hence determine spatial coherence. The route to extracting the spatial coherence length,  $l_{sc}$ , is also illustrated.

showing that after spatial filtering of an OLED, clear fringes can be obtained, but they do not directly measure the spatial coherence of the OLED. Similarly, Saxena et al. followed this method to investigate the spatial coherence from a tris-(8-hydroxyquinoline) aluminum ( $\text{Alq}_3$ )-based OLED. However, a limitation of these studies is that they measured the spatial coherence properties of a spatially filtered OLED, rather than the light source itself.

In this paper, we report measurements of the intrinsic spatial coherence length of a range of OLEDs by introducing a Fourier transform imaging system, i.e. a  $4f$  system. To improve the low visibility of the fringe from the OLEDs, we laterally integrated the OLEDs with external diffractive optical elements (DOEs) that consisted of submicrometer-scale gratings fabricated by UV-nanoimprint lithography (UV-NIL).

## 2. Methods and devices

### 2.1. The optical setup and the method to extract the spatial coherence length

Scheme 1 illustrates the optical setup for measuring the spatial coherence of a light source. The light source was located in the focal plane of the objective lens. In order to have the best detection system for light of low coherence, we combined a double slit ( $125 \mu\text{m}$  separation) with a telescope with  $40\times$  magnification factor that will be able to detect the interference fringes of a light source having a spatial coherence length on the several- $\mu\text{m}$  scale. A cooled CCD camera (SBIG,  $3326 \times 2504$  pixels and  $5.4 \times 5.4 \mu\text{m}^2$

each pixel) was used to capture the fringes. We performed tests to verify the response of our experiment to a wide range of degrees of spatial coherence. To do this we replaced the OLED (see Scheme 1) by a He-Ne laser illuminating a rotating diffuser coated with varying numbers of layers of scattering films (sticky tape). The beam of the He-Ne laser was expanded by a  $60\times$  objective lens and then collimated by incorporating another lens with a focal length of 150 mm. A variable single slit was inserted between the rotating diffuser and the collimating lens to control the beam size. Figure 1a shows the fringes of the light beam passing through a rotating diffuser that consists of 2 outer sticky films (tesafilm) /glass/2 inner sticky films. No clear interference pattern can be observed in Fig. 1a as the phase of the laser beam was completely scrambled by the rotating diffuser. In contrast, the light beam from the He-Ne laser without passing through the diffuser exhibits very clear interference patterns. We used a two-dimensional fast Fourier transform (2D-FFT) to determine and average the visibility of the fringes from our low-coherence light sources. In Fig. 1c, the fringe visibility was plotted by changing the number of sticky films attached to the glass and adjusting the opening of the variable single slit. Using this apparatus, very low visibility (defined in section 2.4) down to 0.02 can be measured.

### 2.2. OLED fabrication and characterization

OLEDs with an iridium (Ir) complex were fabricated by thermal evaporation on glass substrates and with a europium (Eu) complex were processed by

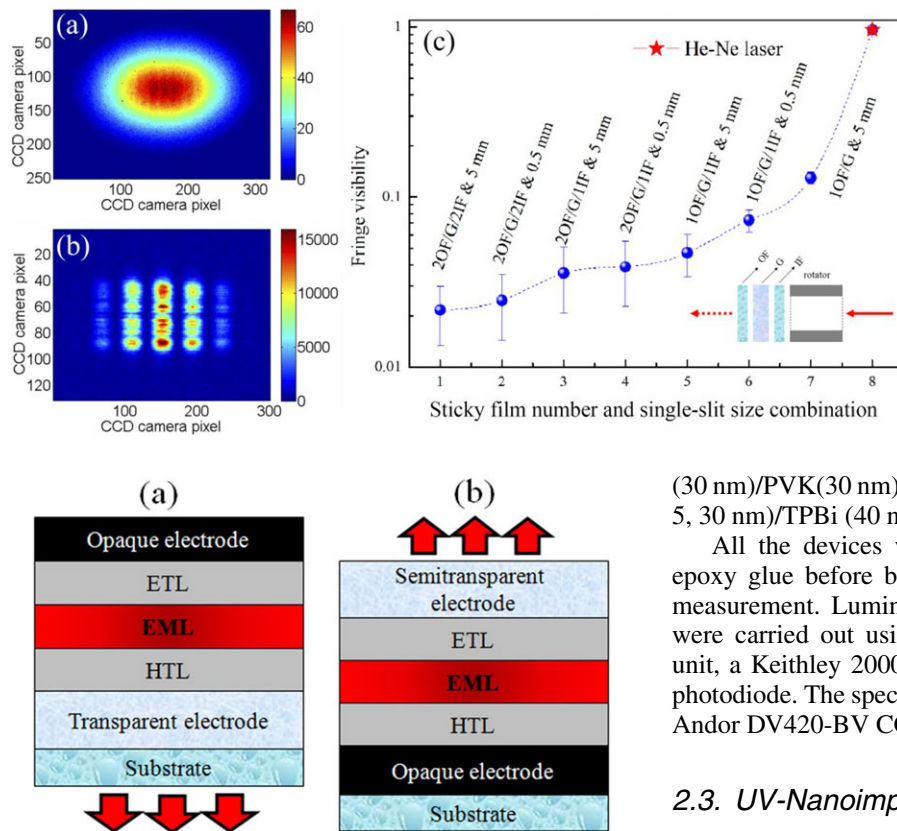


**Figure 1** Fringes captured by the CCD camera (a) with 2 outer films/glass/2 inner films as the rotating diffuser and (b) without the diffuser. (c) Fringe visibility changes with different rotating diffuser used. The outer film (OF), glass (G), the inner film (IF) relative to the rotating diffuser's position (see the inset) and the opening size of the single slit are also indicated.

**Figure 2** The architectures of bottom- (a) and top-emitting (b) OLEDs.

spin coating of the organic layers and evaporation of the electrodes. The structure of our bottom-emitting OLED (shown in Fig. 2a) with an Ir emitter was glass/ITO p-doped HTL(30 nm)/N,N'-di(naphthalene-2-yl)-N,N'-diphenyl-benzidine ( $\alpha$ -NPD, 10 nm)/ $\alpha$ -NPD doped with 10 wt% iridium(III) bis(2-methyl-dibenzo-[f,h]chinoxalin)(acetylacetonate) (Ir(MDQ)<sub>2</sub>(acac), 20 nm)/bis-(2-methyl-8-quinolinolato)-4-(phenyl-phenolato) aluminum(III) (BALq<sub>2</sub>, 10 nm)/n-doped ETL (40 nm)/Al (100 nm). HTL and ETL denote hole- and electron-transporting layers, respectively. The architecture of the top-emitting OLED (shown in Fig. 2b) with the Ir emitter was glass/Al (40 nm)/Ag (40 nm)/p-doped HTL (50 nm)/ $\alpha$ -NPD doped with 10 wt% Ir(MDQ)<sub>2</sub>(acac) (10 nm)/BALq<sub>2</sub> (10 nm)/n-doped ETL (40 nm)/Al (1 nm)/Ag (18 nm).

The structure of the bottom-emitting Eu emitter was similar to that of the devices with an Ir emitter, i.e. glass/ITO/poly(3,4-ethylenedioxythiophene):poly(styrenesulfonate) (PEDOT:PSS, 30 nm)/poly(N-vinylcarbazole) (PVK, 30 nm)/4,4'-N,N'-dicarbazole-biphenyl (CBP):2-(tert-butylphenyl)-5-biphenyl-1,3,4-oxadiazole (PBD):tris(dibenzoylmethane)mono (4,7-diphenylphenanthroline)europium(III) (Eu(DBM)<sub>3</sub>Bphen) (65:30:5, 30 nm)/1,3,5-tris(2-N-phenylbenzimidazolyl)benzene (TPBi, 40 nm)/Ca (20 nm)/Al (100 nm). The top-emitting OLED stack with the Eu emitter was glass/Ag (80 nm)/ PEDOT:PSS

(30 nm)/PVK(30 nm)/CBP:PBD:Eu(DBM)<sub>3</sub>Bphen (65:30:5, 30 nm)/TPBi (40 nm)/Ca (2 nm)/Ag (18 nm).

All the devices were encapsulated with UV-curable epoxy glue before being taken out of the glove-box for measurement. Luminance-current-voltage measurements were carried out using a Keithley 2400 source measure unit, a Keithley 2000 multimeter and a calibrated silicon photodiode. The spectrum was collected by a fiber-coupled Andor DV420-BV CCD spectrometer.

### 2.3. UV-Nanoimprint lithography (UV-NIL)

UV-NIL was used to make large-area micrometer and nanometer scale patterns [33]. Before transferring a thick layer of perfluoropolyether(PFPE)-urethane dimethacrylate (Fluorolink MD700) as a compliant material onto a clean and bare silicon substrate, an adhesive layer of (3-Trimethoxysilyl)propyl acrylate (Sigma-Aldrich) was spin coated directly onto the glass substrate after oxygen plasma treatment. Another layer of MD700 was spin coated on the glass substrate after UV exposure for 220 s. Through the second UV exposure, the 1D grating pattern with a period of 350 nm on a Si master was transferred onto this glass substrate (daughter stamp) by adding some droplets of perfluoroalkylpolyether (Fluorolink MD500) mixed with 1–2% of the photoinitiator DURACOUR.

The daughter stamp was used as a mold for replicating the grating structures onto a photoresist (Micro Resist Technology UVCur06) that was spin coated atop another bare glass substrate with an additional adhesion promoter (Micro Resist Technology mr-APS1). The UV nanoimprint lithography (UV-NIL) processes were performed using an EVG® 620 automated mask alignment system. The grating profile was imaged by a Hitachi S-4800 scanning electron microscope (SEM).

### 2.4. Simulation of the spatial coherence length

In the literature, the spatial coherence length of a light source can usually be estimated qualitatively by the well-known Young's double-slit experiment. The measured fringe visibility of a light source lies from zero to one

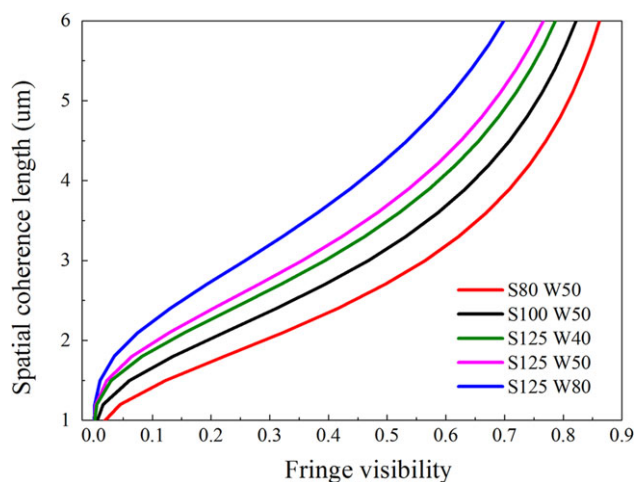


**Figure 3** Simulated spatial coherence length as a function of the fringe visibility, considering different separation ( $S$  in  $\mu\text{m}$ ) and width ( $W$  in  $\mu\text{m}$ ) of the double slit used in the setup shown in Scheme 1.

corresponding to a light source being incoherent to fully coherent. In order to relate the spatial coherence length to the fringe visibility quantitatively, we used a numerical simulation. A partially coherent beam can be described by the Gaussian–Schell model correlator,

$$\mu(\vec{\rho}_1, \vec{\rho}_2) = \exp\left(-|\vec{\rho}_1 - \vec{\rho}_2|^2 / L_c^2\right), \quad (1)$$

where  $\vec{\rho}_1$  and  $\vec{\rho}_2$  are the vectors denoting two different points on the transverse plane that is perpendicular to the beam propagation direction, and  $L_c$  is the transverse coherence length [34]. We then simulate the passage of such a partially coherent beam through any optical system, such as a telescope or a double slit, by propagating the beam with the method of ABCD ray matrices [35]. With this numerical method, we can purposely simulate our optical system as shown in Scheme 1. From the interference pattern, we can calculate the fringe visibility as,

$$V = \frac{I_{\max} - I_{\min}}{I_{\max} + I_{\min}}, \quad (2)$$

where  $I_{\max}$  and  $I_{\min}$  are the peak intensities of the upper and lower envelopes of the measured fringes. For our particular application, we need to modify this equation to calculate the modified fringe visibility due to the high noise level and low visibility. In a similar way to other fringe-analysis techniques, a Fourier transform was applied to the original fringe pattern, and the visibility calculated in the Fourier domain as,

$$V_{\text{FFT}} = \frac{P_1}{P_0}, \quad (3)$$

where  $P_0$  is the area under the zeroth order peak, and  $P_1$  is the sum of the areas under the two first-order peaks in the Fourier domain. The results of the simulation relating

spatial coherence length to fringe visibility are shown in Fig. 3. This figure therefore allows us to deduce the spatial coherence length of an OLED from a measurement of the visibility of fringes in the double-slit experiment.

### 3. Results and discussion

#### 3.1. The electrical and optical properties of the OLEDs

The iridium complex-based bottom-emitting OLED (Ir-BEOLED) exhibited a very low turn-on voltage of 2.1 V at a luminance of 1  $\text{cd}/\text{m}^2$  and a high luminance of 10 000  $\text{cd}/\text{m}^2$  at 4.0 V (see Figs. 4a and b). From Fig. 4c, a full width at half-maximum (FWHM) of the EL spectrum at 1 mA was determined to be 79.4 nm and the peak wavelength was 609 nm. Similarly, the iridium complex-based top-emitting OLED (Ir-TEOLED) has a turn-on voltage of 2.3 V contributed to the use of the electrically doped charge transporting layers [36]. However, the luminance reached 10 000  $\text{cd}/\text{m}^2$  at around 4.8 V ascribed to the different optical cavity effect and outcoupling property, which led to a FWHM of 72.5 nm and peak emission at 625 nm.

Unlike the iridium complex-based devices, the Eu complex-based devices (Eu-BEOLED and Eu-TEOLED) showed much higher driving voltages and lower luminance resulted from less conductive charge transporting layer used (Figs. 5a and b). Nevertheless, this Eu complex exhibited a very narrow emissive bandwidth as a result of the characteristic emission from the  $\text{Eu}^{3+}$  ion based on the  ${}^5\text{D}_0$ – ${}^7\text{F}_2$  transition, which makes it an ideal candidate for the pure red devices [37]. Therefore, we observed small FWHMs of 5.6 nm and 5.5 nm and peak emission both at 611 nm (shown in Fig. 5c), corresponding to Eu-BEOLED and Eu-TEOLED, respectively.

#### 3.2. The spatial coherence measurements of OLEDs

To assess the spatial coherence of the OLEDs, we fixed the OLEDs at the focal plane of the objective lens and captured the fringe with the CCD camera placed at the focal plane of Lens 3 illustrated in Scheme 1. Figures 6a and b show the fringes and 2D-FFT patterns of a reference He-Ne laser without using the rotating diffuser. Very high visibility ( $\sim 1$ ) was observed as the laser has a much higher degree of spatial coherence than the partially coherent light sources. As the normal OLEDs have low coherence, it is somewhat difficult to precisely define the first-order peaks after 2D-FFT. The clear 2D-FFT patterns of the He-Ne laser were therefore used to identify the boundaries of the peaks of the 2D-FFT patterns, using the fact that the peaks have no position shift once the optical setup is fixed. We then calculated the fringe visibility from the ratio of the first order to the zeroth order peak areas after 2D-FFT (Figs. 6d and f) and found it to be  $0.05 \pm 0.01$  for the Ir-BEOLED and  $0.06 \pm 0.01$  for the Eu-BEOLED. For the double slit geometry used (width 40  $\mu\text{m}$ ,

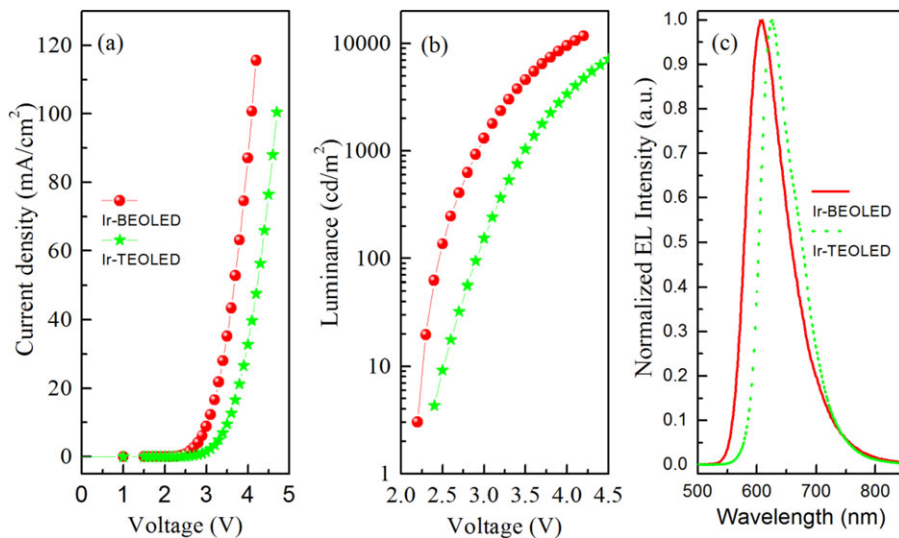


**Figure 4** Current density–voltage (a) and luminance–voltage (b) characteristics and the EL spectrum at 1 mA (c) of the Ir complex-based bottom- and top-emitting OLED (Ir-BEOLED and Ir-TEOLED).

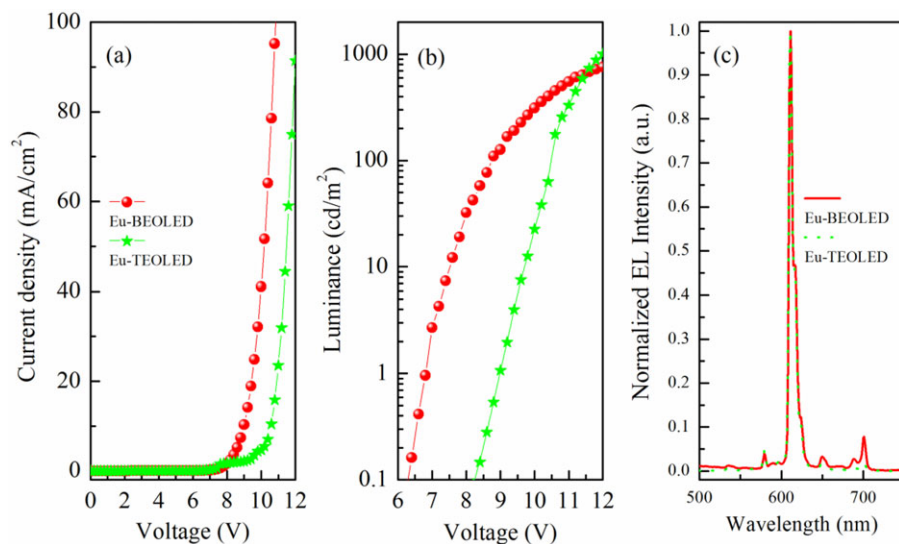


**Figure 5** Current density–voltage (a) and luminance–voltage (b) characteristics and the EL spectrum at 1 mA (c) of the Eu complex-based bottom- and top-emitting OLED (Eu-BEOLED and Eu-TEOLED).

separation  $125 \mu\text{m}$ ) the spatial coherence lengths of Ir- and Eu-BEOLEDs can be deduced from Fig. 3 to be  $1.6 \pm 0.1$  and  $1.7 \pm 0.1 \mu\text{m}$ .

For the top-emitting OLEDs, we obtained visibilities of the fringes (see Figs. 7a and c) of  $0.07 \pm 0.01$  and  $0.11 \pm 0.02$  for the Ir and Eu emitter-based devices, respectively (Figs. 7b and d). Therefore, the top-emitting Ir and Eu emitter-based devices exhibited slightly enhanced spatial coherence lengths of  $1.73 \pm 0.06$  and  $1.9 \pm 0.1 \mu\text{m}$ , compared to the bottom-emitting counterparts. The lower visibility of the Ir complex-based devices arises from their broader emission spectrum, which leads to overlapping fringe patterns for different wavelengths.

### 3.3. Structuring the spatial coherence of BEOLEDs with a DOE

To manipulate the light beams from OLEDs for phase control, we need to increase the spatial coherence. Theoretical

studies have established that under certain conditions metallic gratings may improve the spatial coherence through the excitation of surface plasmon polaritons [38]. Other studies have shown that gratings can be embedded into the emitting layer of an OLED and lead to a strongly modified angular emission pattern [39]. However, it is challenging to produce uniform and stable devices with the gratings inside an OLED. Figure 8a shows the average mode contributions of the BEOLED and TEOLED calculated using standard methods [40, 41]. It is clear that a large portion ( $\sim 18\%$ ) of the light is trapped in the glass substrate of the BEOLED. On the contrary, there is no substrate mode in a TEOLED as a metallic anode is used as the bottom contact. Here, we constructed a simple scheme to extract the substrate modes from the BEOLED by laterally integrating a DOE adjacent to the glass substrate (thickness 1 mm) (see Fig. 8b) following the approach in reference 39. The grating-based DOE scatters out substrate modes, and was fabricated by UV-NIL with an additional 20-nm thick Ag layer deposited on top of the NIL resist to enhance the scattering efficiency.

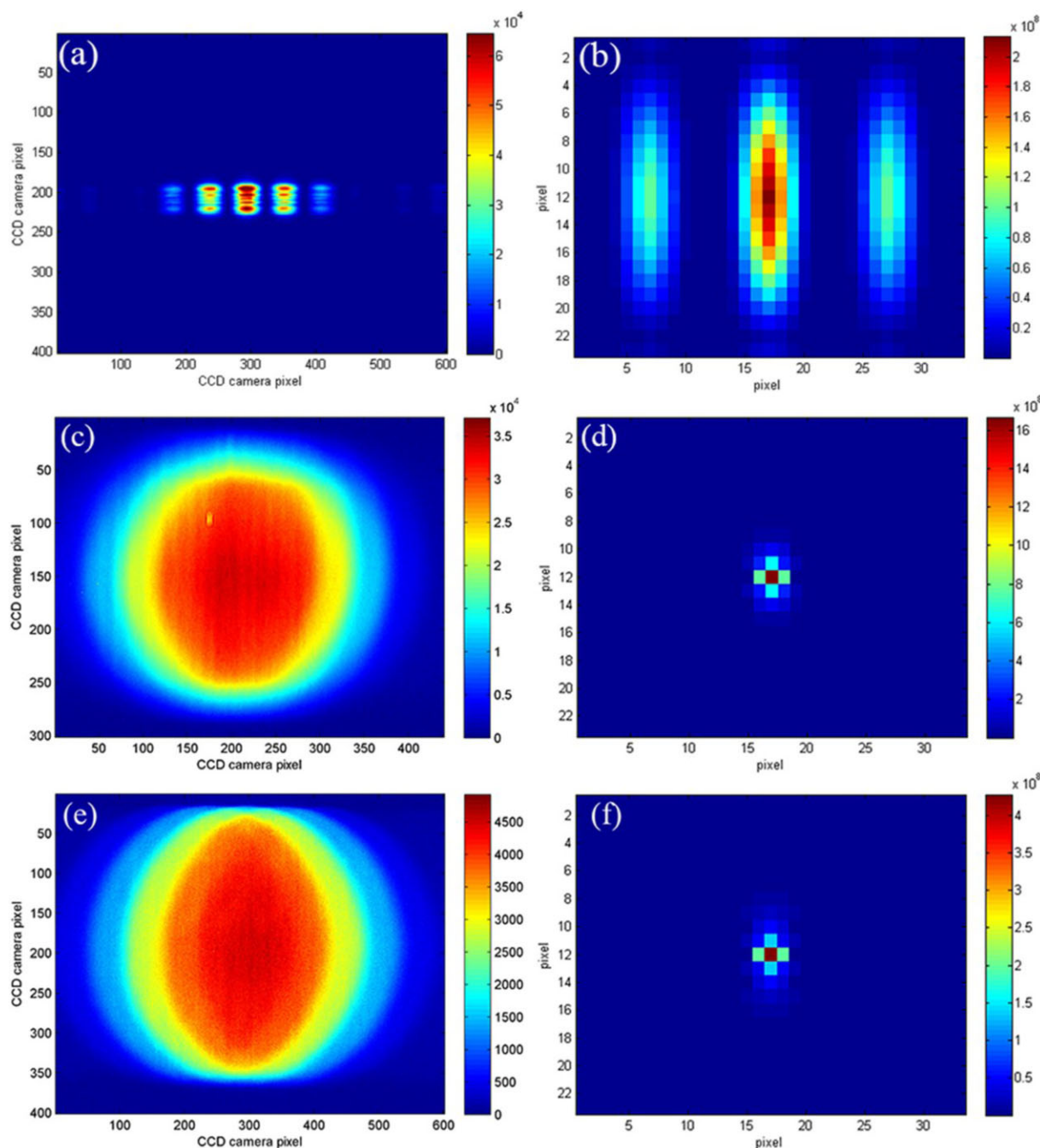


**Figure 6** Fringes of He-Ne laser (a), Ir-BEOLEDs (c) and Eu-BEOLED (e). 2D-FFT Patterns of the fringes of He-Ne laser (b), Ir-BEOLEDs (d) and Eu-BEOLED (f).

To characterize the spatial coherence, the emission from the DOE was coupled into the telescope (see Scheme 1) and the fringes of iridium and europium complex-based devices captured by the CCD camera are plotted in Figs. 9a and c. This gave by far the clearest interference patterns of the devices studied in this paper. The fringe visibility of Ir and Eu complex-based BEOLEDs were  $0.20 \pm 0.03$  and  $0.34 \pm 0.04$ , respectively.

Using the 2D-FFT (shown in Figs. 9b and d) and combining the numerical simulation, we extract spatial coherence lengths of  $2.28 \pm 0.06 \mu\text{m}$  and  $2.8 \pm 0.1 \mu\text{m}$  for the Ir and Eu complexes, respectively. A detailed study of this effect is outside the scope of this paper but it is encouraging that the corresponding devices with DOE gave more than 60% improvement of the spatial coherence length.

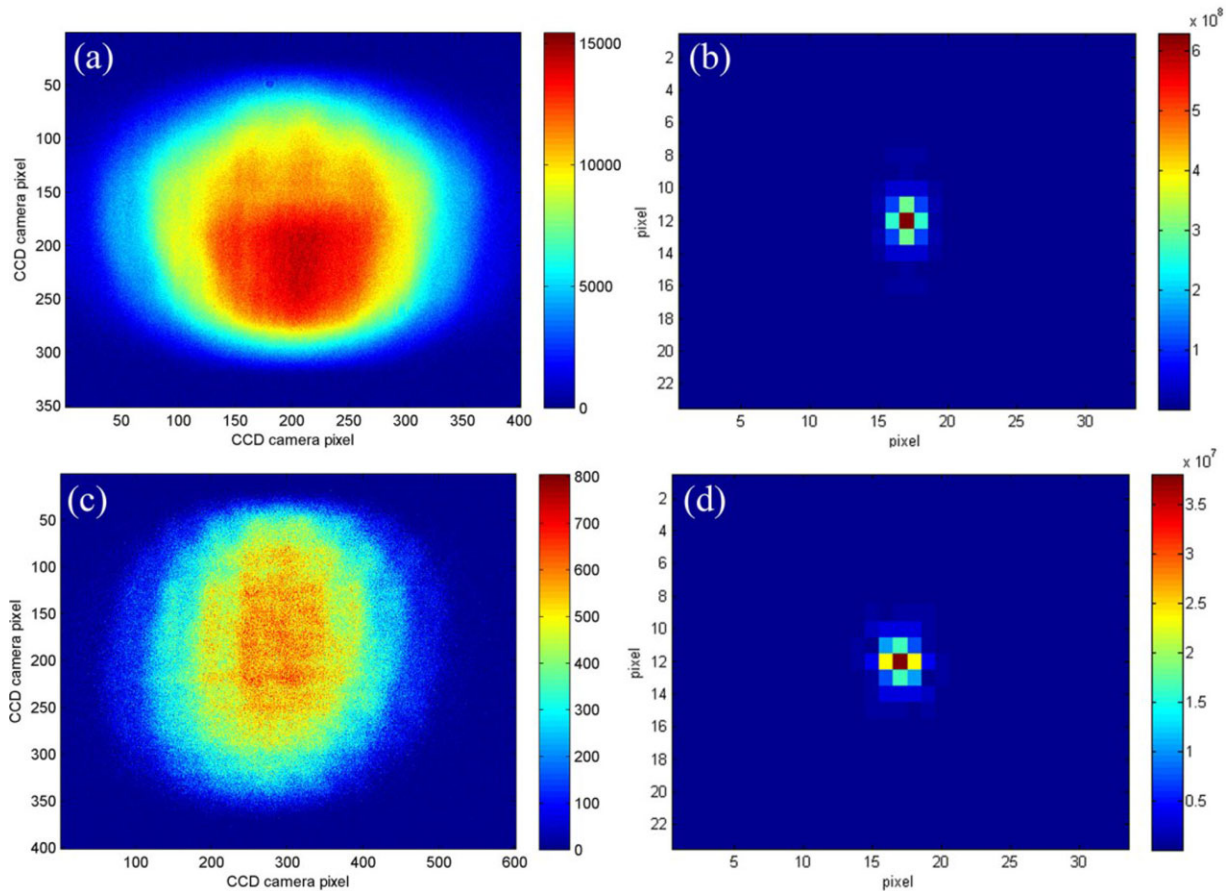


**Figure 7** Fringes of TEOLEDs based on Ir (a) and Eu (c) complexes as the emitters. (b) and (d) are the corresponding 2D-FFT patterns.

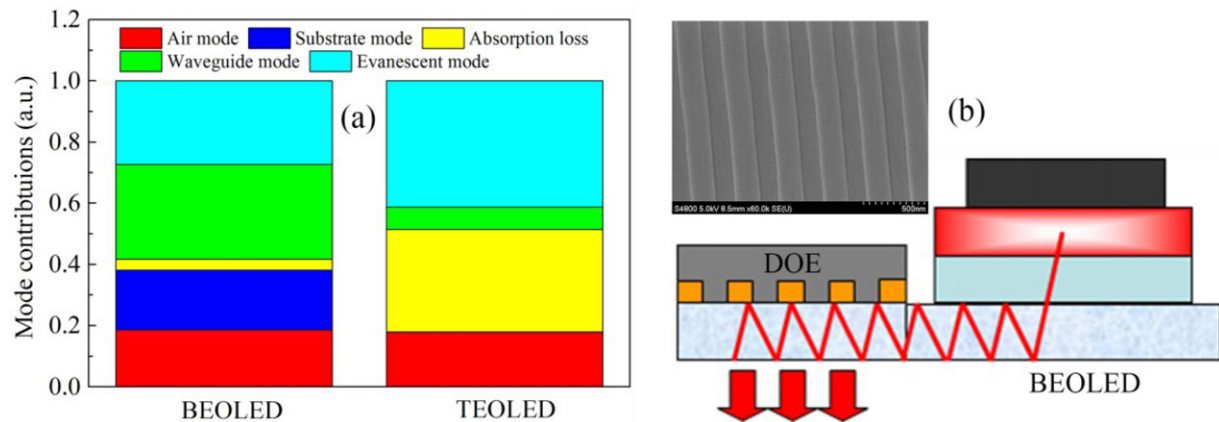


**Figure 8** (a) Comparison of the calculated optical-mode contributions of BEOLED and TEOLED. (b) The schematic diagram of the laterally integrated BEOLED and DOE and the outcoupled light beams for the spatial coherence measurement. The inset above the DOE is an SEM image of the grating on the glass substrate.

#### 4. Conclusion and outlook

We have constructed an optical setup composed of a telescope and a Young's double slit to determine the spatial coherence of OLEDs. This was used to perform a *quan-*

*titative* investigation of the spatial coherence lengths of OLEDs. We showed that by integrating diffractive optical elements with bottom-emitting OLEDs, we could manipulate the spatial coherence from the organic light sources. As shown in Fig. 10, we observed that the fringe

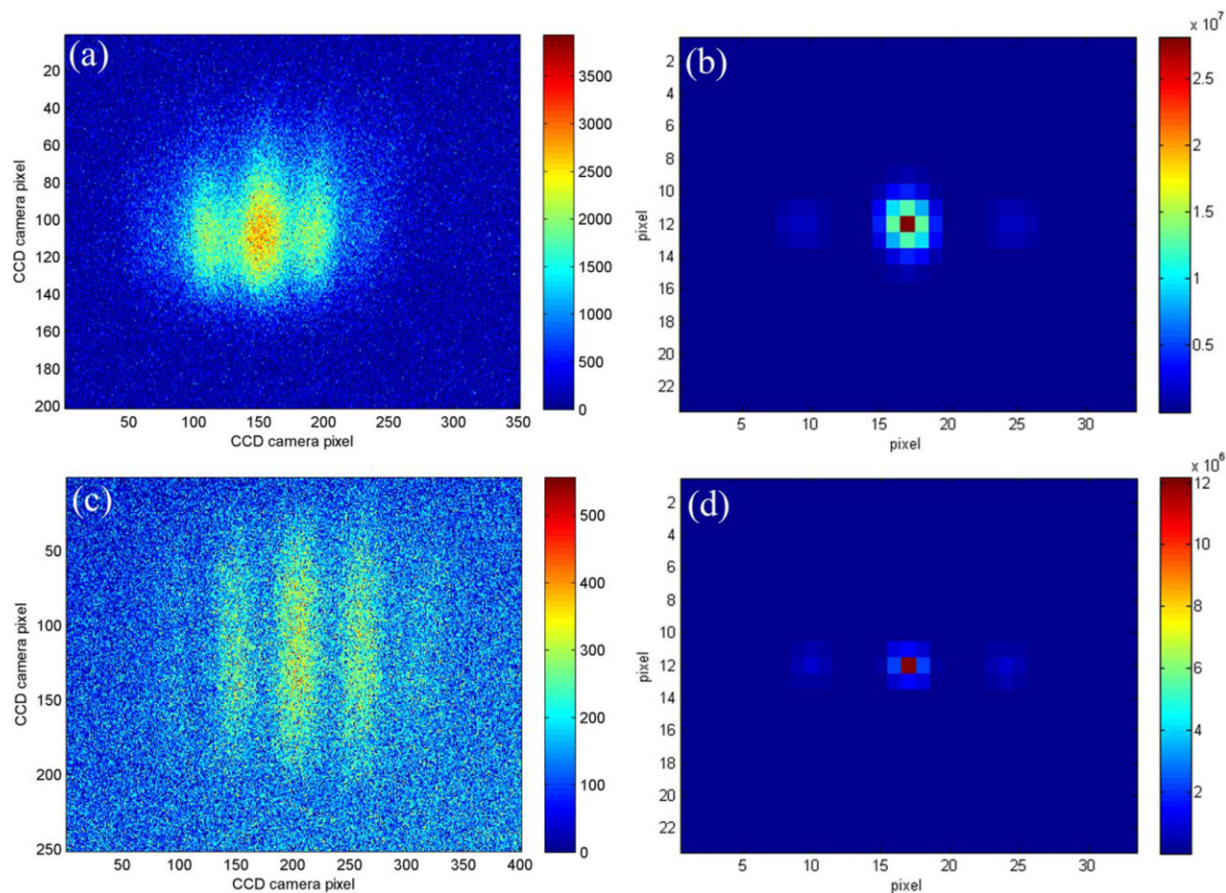


**Figure 9** Fringes of the emission from DOE connected to BEOLEDs based on Ir (a) and Eu (b) complexes as the emitters.

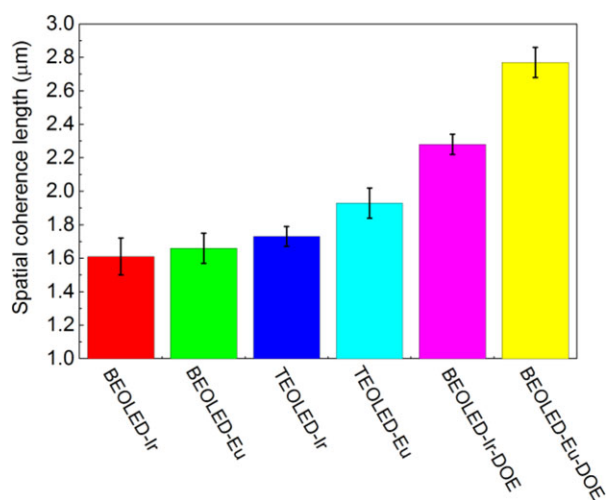


**Figure 10** Summary of the spatial coherence lengths of OLEDs measured using the double slit experiment.

visibility was gradually improved from 0.05 to 0.34. Due to the broad emission of the Ir complex, the devices exhibited relatively low fringe visibility and thus small spatial coherence lengths with weak microcavity effect. The spatial coherence lengths of a europium complex-based OLED

was improved from  $\sim 1.7$  to  $\sim 1.9 \mu\text{m}$  by changing the stack architecture from bottom emitting to top emitting. Another 44% improvement can be achieved by employing an external DOE. In the future it should be possible to achieve higher spatial coherence by deliberately coupling out an individual optical mode with a suitable grating structure. Our results pave a novel path for optical management in organic light sources for visible-light communication and biomedical applications.

**Acknowledgements.** This work was supported by the Engineering and Physical Science Research Council (EPSRC) grants “Challenging the limits of photonics: structured light” EP/J01771X and “Ultra-parallel visible light communications” EP/K00042X. IDWS and KD also acknowledge Royal Society Wolfson Research Merit awards. The research data supporting this paper can be accessed at <http://dx.doi.org/10.17630/73b69cb8-ba6c-4d71-9985-e723e932c337>.

**Received:** 15 March 2015, **Revised:** 17 September 2015,  
**Accepted:** 28 September 2015

**Published online:** 30 November 2015

**Key words:** OLED, double-slit experiment, spatial coherence length, diffractive optical element.



## References

- [1] S. Reineke, F. Lindner, G. Schwartz, N. Seidler, K. Walzer, B. Lussem, and K. Leo, *Nature* **459**, 234–238 (2009).
- [2] G. Xie, Q. Xue, P. Chen, C. Tao, C. Zhao, J. Lu, Z. Gong, T. Zhang, R. Huang, H. Du, W. Xie, J. Hou, Y. Zhao, and S. Liu, *Org. Electron.* **11**, 407–411 (2010).
- [3] J. Blochwitz-Nimoth, O. Langguth, S. Murano, G. He, T. Romainczyk, and J. Birnstock, *Journal of the Society for Information Display*, **18**, 596–605 (2010).
- [4] C. Adachi, M. A. Baldo, M. E. Thompson, and S. R. Forrest, *J. Appl. Phys.* **90**, 5048–5051 (2001).
- [5] R. H. Friend, R. W. Gymer, A. B. Holmes, J. H. Burroughes, R. N. Marks, C. Taliani, D. D. C. Bradley, D. A. D. Santos, J. L. Bredas, M. Logdlund, and W. R. Salaneck, *Nature* **397**, 121–128 (1999).
- [6] J. Kido, M. Kimura, and K. Nagai, *Science* **267**, 1332–1334 (1995).
- [7] C. W. Tang and S. A. VanSlyke, *Appl. Phys. Lett.* **51**, 913–915, (1987).
- [8] M. A. Baldo, D. F. O'Brien, Y. You, A. Shoustikov, S. Sibley, M. E. Thompson, and S. R. Forrest, *Nature* **395**, 151–154 (1998).
- [9] X. Gong, S. Wang, D. Moses, G. C. Bazan, and A. J. Heeger, *Adv. Mater.* **17**, 2053–2058 (2005).
- [10] H. T. Nicolai, A. Hof, and P. W. M. Blom, *Adv. Funct. Mater.* **22**, 2040–2047 (2012).
- [11] C.-W. Chen, Y.-J. Lu, C.-C. Wu, E. H.-E. Wu, C.-W. Chu, and Y. Yang, *Appl. Phys. Lett.* **87**, 241121 (2005).
- [12] F. A. Boroumand, P. W. Fry, and D. G. Lidzey, *Nano Lett.* **5**, 67–71 (2005).
- [13] P. L. Burn, S. C. Lo, and I. D. W. Samuel, *Adv. Mater.* **19**, 1675–1688 (2007).
- [14] S. C. Lo, N. A. H. Male, J. P. J. Markham, S. W. Magennis, P. L. Burn, O. V. Salata, and I. D. W. Samuel, *Adv. Mater.* **14**, 975–979 (2002).
- [15] P. A. Haigh, Z. Ghassemlooy, H. Le Minh, S. Rajbhandari, F. Arca, S. F. Tedde, O. Hayden, and I. Papakonstantinou, *J. Lightwave Technol.* **30**, 3081–3088 (2012).
- [16] R. M. Owens and G. G. Malliaras, *MRS Bull.* **35**, 449–456 (2010).
- [17] J.-C. G. Bünzli, S. Comby, A.-S. Chauvin, and C. D. B. Vandevyver, *J. Rare Earths* **25**, 257–274 (2007).
- [18] S. K. Attili, A. Lesar, A. McNeill, M. Camacho-Lopez, H. Moseley, S. Ibbotson, I. D. W. Samuel, and J. Ferguson, *Brit. J. Dermatol.* **161**, 170–173 (2009).
- [19] K. Walzer, B. Maennig, M. Pfeiffer, and K. Leo, *Chem. Rev.* **107**, 1233–1271 (2007).
- [20] G. M. Farinola and R. Ragni, *Chem. Soc. Rev.* **40**, 3467–3482 (2011).
- [21] Y. Shirota and H. Kageyama, *Chem. Rev.* **107**, 953–1010 (2007).
- [22] D. P. Puzzo, M. G. Helander, P. G. O'Brien, Z. Wang, N. Soheilnia, N. Kherani, Z. Lu, and G. A. Ozin, *Nano Lett.* **11**, 1457–1462 (2011).
- [23] C.-L. Lin, H.-W. Lin, and C.-C. Wu, *Appl. Phys. Lett.* **87**, 021101 (2005).
- [24] J. R. Tischler, M. S. Bradley, V. Bulović, J. H. Song, and A. Nurmikko, *Phys. Rev. Lett.* **95**, 036401 (2005).
- [25] V. Bulović, V. B. Khalfin, G. Gu, P. E. Burrows, D. Z. Garbuzov, and S. R. Forrest, *Phys. Rev. B* **58**, 3730–3740 (1998).
- [26] S. Tokito, T. Tsutsui, and Y. Taga, *J. Appl. Phys.* **86**, 2407–2411 (1999).
- [27] N. Christogiannis, N. Somaschi, P. Michetti, D. M. Coles, P. G. Savvidis, P. G. Lagoudakis, and D. G. Lidzey, *Adv. Opt. Mater.* **1**, 503–509 (2013).
- [28] T. Berki, P. Németh, and J. Hegedüs, *Lasers Med. Sci.* **3**, 35–39 (1988).
- [29] D. Fixler, H. Duadi, R. Ankri, and Z. Zalevsky, *Lasers Surg. Med.* **43**, 339–343 (2011).
- [30] H. Subramanian, P. Pradhan, Y. L. Kim, and V. Backman, *Phys. Rev. E* **75**, 041914 (2007).
- [31] F. J. Duarte, L. S. Liao, and K. M. Vaeth, *Opt. Lett.* **30**, 3072–3074 (2005).
- [32] K. Saxena, D. S. Mehta, R. Srivastava, and M. N. Kamalasanan, *Appl. Phys. Lett.* **89**, 061124 (2006).
- [33] G. Tsiminis, Y. Wang, A. L. Kanibolotsky, A. R. Inigo, P. J. Skabara, I. D. W. Samuel, and G. A. Turnbull, *Adv. Mater.* **25**, 2826–2830 (2013).
- [34] Y. Yang, M. Chen, M. Mazilu, A. Mourka, Y. Liu, and K. Dholakia, *New J. Phys.* **15**, 113053 (2013).
- [35] P. A. Bélanger, *Opt. Lett.* **16**, 196–198 (1991).
- [36] G. Xie, K. Fehse, K. Leo, and M. C. Gather, *Org. Electron.* **14**, 2331–2340 (2013).
- [37] T. W. Canzler and J. Kido, *Org. Electron.* **7**, 29–37 (2006).
- [38] T. Saastamoinen and H. Lajunen, *Opt. Lett.* **38**, 5000–5003 (2013).
- [39] S. Zhang, G. A. Turnbull, and I. D. W. Samuel, *Appl. Phys. Lett.* **103**, 213302 (2013).
- [40] R. R. Chance, A. Prock, and R. Silbey, *Adv. Chem. Phys.* **137**, 16 (1978).
- [41] P. Yeh, *Optical Waves in Layered Media*, (John Wiley & Sons, New York 1988).